Glacial aerodynamic roughness estimates: uncertainty, sensitivity and precision in field measurements

Joshua R Chambers[1], Mark W Smith[1], Duncan J Quincey[1], Jonathan L Carrivick[1], Andrew N Ross[2], Mike R James[3]

[1]School of Geography, University of Leeds, Leeds, LS2 9JT

[2]School of Earth and Environment, University of Leeds, Leeds, LS2 9JT

[3]Lancaster Environment Centre, Lancaster University, Lancaster, LA1 4YQ

Corresponding author: Joshua Chambers (gyjrc@leeds.ac.uk)

Key Points:

- Sensitivities and uncertainties in glacial aerodynamic roughness reviewed and analyzed using new field data
- Wind profile and microtopographic methods provide realistic values of z_0 in absence of more robust eddy covariance data
- Despite scale/resolution dependency, microtopographic estimates show good agreement with profiles and could be used to upscale studies.

Abstract

Calculation of the sensible and latent heat (turbulent) fluxes is required in order to close the surface energy budget of glaciers and model glacial melt. The aerodynamic roughness length, z_0, is a key parameter in the bulk approach to calculating sensible heat flux; yet, z_0 is commonly considered simply as a tuning parameter or generalized between surfaces and over time. Spatially and temporally distributed observations of z_0 over ice are rare. Both direct (from wind towers and sonic anemometers) and indirect (from microtopographic surveys) measurements of z_0 are subject to sensitivities and uncertainties that are often unstated or overlooked. In this study, we present a quantitative evaluation of aerodynamic profile-based and microtopographic methods and their effect on z_0 using data collected from Storglaciären and Sydöstra Kaskasatjäkkaglaciären, Tarfala Valley, Arctic Sweden. Aggressive data filters discard most of the wind tower data, but still produce realistic z_0 values of 1.9 mm and 2 mm. Despite uncertainty introduced by scale and resolution dependence, microtopographic methods produced estimates of z_0 comparable to wind tower values and those found on similar surfaces. We conclude that: 1) in the absence of direct turbulent flux measurements from sonic anemometers, the profile and microtopographic methods provide realistic z_0 values, 2) both 2D and 3D microtopographic methods are dependent on scale, resolution, and the chosen detrending method, and 3) careful calibration of these parameters could enable glacier-wide

This article has been accepted for publication and undergone full peer review but has not been through the copyediting, typesetting, pagination and proofreading process which may lead to differences between this version and the Version of Record. Please cite this article as doi: 10.1029/2019JF005167

investigations of z_0 from remotely sensed data, including those increasingly available from satellite platforms.

1. Introduction

At local and regional scales, surface energy balance modelling is commonly used to calculate glacier melt and contribution to stream flow (Hock, 2005), wherein sensible and latent heat (turbulent) fluxes are usually secondary to the net radiative energy fluxes. The contribution of the turbulent fluxes is enhanced during conditions when radiative fluxes are reduced, e.g. in cloudy, windy conditions and in maritime climates (Anderson *et al.*, 2010; Giesen *et al.*, 2014), and have been recently implicated in widespread melt events on the Greenland Ice Sheet, for example, during which >98% of the ice surface experienced melt (Fausto *et al.*, 2016). As changes in cyclonic activity (Gorter *et al.*, 2014) and precipitation rates (Vavrus, 2013) are likely to increase the significance of the turbulent fluxes, it is imperative to ensure that they are calculated as accurately as possible so that current levels of melt can be quantified and future melt can be forecast confidently.

Three main methods for calculating turbulent fluxes over glacier surfaces exist: eddy correlation (EC), the profile method, and the bulk aerodynamic method (Fig. 1). EC uses sonic anemometers to record the three-dimensional (3D) movement of air in turbulent eddies (Burba, 2013) and, being the closest to a direct measurement of the turbulent fluxes, is often used as the benchmark for validating the two alternative theoretical model-based methods below (Munro, 1989; Greuell and Genthon, 2004). A number of aspects, including the cost of the sensors (typically > £10000) and their unsuitability for long observational periods in harsh arctic and alpine climates, make EC impractical for most glacial energy balance studies. The profile method estimates turbulent fluxes from near-surface interpolated profiles of wind speed, air temperature and specific humidity (Garratt, 1992). The bulk approach requires measurements of each from only one level, as are typically available from a standard meteorological station, assuming that the aerodynamic roughness length (z_0) and surface temperature are known. This study focuses on the parameterisation of z_0 for the bulk approach (Fig. 1; orange boxes), as the comparatively low requirement for data collection makes it a popular choice in energy balance studies (e.g. Favier *et al.*, 2004; Arnold *et al.*, 2006; Brock *et al.*, 2010; Bravo *et al.*, 2017; Litt *et al.*, 2017; Radić *et al.*, 2017).

The aerodynamic roughness length, z_0, is the height above a surface where wind speed becomes zero, controlled by the geometry of the surface (Stull, 1988). z_0 is difficult to measure directly (usually in the order of mm over glaciers) and several different ways of obtaining a value exist; many glacial energy balance studies following the bulk approach use values from elsewhere in the literature, or use z_0 as a parameter to tune models to fit observed melt (e.g. Inoue and Yoshida, 1980; Braun and Hock, 2004; Arnold et al., 2006; Fausto et al., 2016; Bravo et al., 2017). Often, z_0 is erroneously assumed to be spatially and temporally uniform, in contradiction of observations (c.f. Brock et al., 2006).

Aerodynamic profiles are traditionally used to find z_0 (Hock and Holmgren, 1996; Brock *et al.*, 2006; Sicart *et al.*, 2014; Quincey *et al.*, 2017) however, they are subject to large uncertainties and sensitivities, and provide point data. The use of microtopographic transects is commonly used to circumvent the need for wind towers, enabling more rapid, spatially

distributed z_0 estimates (Munro, 1989; Brock *et al.*, 2006; Irvine-Fynn *et al.*, 2014; Smith *et al.*, 2016a; Miles *et al.*, 2017). However, the calculation of z_0 from microtopographic transects is subject to a number of assumptions surrounding the spacing and dimension of roughness elements, shading and sheltering and the effects of wind direction (Smith *et al.*, 2016a) which are unrealistic, but largely ignored in the absence of a more robust approach.

Recently, fine-resolution survey techniques such as Structure from Motion (SfM) photogrammetry and terrestrial laser scanning (TLS) have been explored for their ability to enhance glacier surface microtopographic data collection. These methods have been used to collect transects rapidly and at fine resolution (Miles *et al.*, 2017), and to devise 3D geometric approaches to finding z_0 that relax the previously mentioned assumptions (see Section 2.2), including initial steps towards glacier-wide z_0 maps (Smith *et al.*, 2016a) and calculating z_0 from remotely sensed data products (Fitzpatrick *et al.*, 2019). Potential for cryosphere-wide z_0 measurements increases in line with the expansion of available fine-resolution data sources (e.g. ArcticDEM, global DEM, NASA High Mountain Asia DEM).

As a first step, we seek here to explore the existing methods for finding z_0 from wind profiles and microtopography, and to understand their sensitivities and uncertainties. The aim of this paper is to test existing methods as a foundation for the development of new methods in future work. We present a brief review of the methods that are currently available, highlighting factors that can alter z_0 unrelated to variability in the physical properties being measured. These critical uncertainties are summarized at the end of Sections 2.1 and 2.2. Then, using new data collected from two glaciers, Storglaciären and Sydöstra Kaskasatjäkkaglaciären in Arctic Sweden (Section 3), we present quantitative analysis of the uncertainties in Sections 4.1 and 4.2

2. Previous work

2.1 Aerodynamic profile z_0

In the field, the aerodynamic profile method (based on Monin-Obukhov (MO) similarity theory (Foken, 2006)) can be used to capture site specific z_0 values for use with the bulk approach. For simplicity we shorten this to the 'profile method', and use 'profile z_0' to refer to z_0 obtained in this manner. The profile method is only valid for near neutral conditions, and is used to extrapolate z_0 from linear least-squares fits of wind speed, profiles of which are assumed to be log-linear above a surface (Garratt, 1992). Wind velocity (U, m s^{-1}) at height z (m) is given by

$$U(z) = \frac{u_*}{\kappa}\left(\ln\frac{z}{z_0} + \alpha_m \frac{z}{L}\right), \quad (2)$$

where u_* is the wind velocity scale (m s^{-1}), k is the von Karman constant (κ = 0.4). $\alpha_m z/L$ is a stability function within which α_m is an empirically derived coefficient (α_m = 5) (Dyer and Hicks, 1970; Stull, 1988) and L is the Obukhov length (the height at which buoyant production of turbulent kinetic energy equals shear production (Foken, 2006)). This correction can be used to extend the validity of the method to weak-to-moderate stabilities. L can be calculated directly from sonic anemometer measurements, or inferred by iteratively fitting wind speed and temperature profiles (e.g. Quincey *et al.*, 2017). Briefly, the method involves making an initial

guess at L (in this case 10^8 m, implying effectively neutral conditions). From this, log-linear profiles can be fitted to the wind and temperature data. This gives values for z_0, u^* and T^* (temperature scale, °C), from which a new (more accurate) value of L can be calculated. This process is repeated until the values of L converge or until some limit is reached, in which case it is assumed that the profiles do not fit the theory and so the profiles are not used to calculate z_0. Wind speed and temperature profiles obtained from mast-mounted cup anemometers and shielded/vented thermometers facing perpendicular to the prevailing wind are commonly used in this approach (e.g. Smeets *et al.*, 1998, 1999; Brock *et al.*, 2006; Pelletier and Field, 2016).

MO similarity theory has underpinned turbulent flux calculations in studies of the surface-atmosphere boundary layer since its conception in 1954 (Monin and Obukhov, 1954; Stull, 1988; Foken, 2008). However, the theory does not necessarily hold over glacial surfaces (Denby and Greuell, 2000; Litt *et al.*, 2014; Radić *et al.*, 2017). Low surface temperatures on glaciers cool the air near the surface, inducing density driven katabatic (glacier) winds (Denby and Greuell, 2000; Denby and Smeets, 2000) and creating strongly stable conditions with a wind speed maximum within the first few metres above the surface. These conditions therefore violate a number of key assumptions made by MO similarity theory: that there is atmospheric stationarity, low advection and a constant flux layer. This makes MO similarity theory only representative of a very thin layer above the ice surface, thus turbulent flux measurements made above the surface are disconnected from their surface values (Denby and Greuell, 2000). Nonetheless, MO similarity theory is often applied in glacier studies because of a lack of alternative (Denby, 1999; Stiperski and Rotach, 2016; Radić *et al.*, 2017).

Where the profile method is used for estimating z_0, measured wind velocity and air temperature profiles are compared with ideal log-linear profiles, and those with a coefficient of determination which is too low (e.g. r^2 <0.98) are discarded. Additional filters can reject: i) data with wind speeds less than cup anemometer stall speeds; ii) non-stationary conditions; and iii) data from specific wind directions (Andreas *et al.*, 2010). These filters drastically reduce the amount of data by up to 98% (Miles *et al.*, 2017); that reduction is a reflection of how rarely the assumptions of the profile method are met.

MO breaks down in very stable or unstable conditions. In moderately stable/unstable conditions, MO similarity theory introduces an empirical stability correction to the wind (and temperature) profiles, which depends on the ratio of the height above the ground, z, to the Obukhov length, L. The stability correction has been shown to be valid for $-5 < z/L < 1$ (Garratt, 1992). L can be determined iteratively as described earlier. As a result, a z_0 value is obtained for each time-step, which can then be averaged or used to examine the temporal change in z_0. Data are typically averaged over periods of up to 30 minutes to ensure an appropriate number of turbulent eddies are samples, which can mask more subtle temporal dynamics in z_0 – a restriction which is lifted with microtopographic approaches.

Regardless of the slope of the glacier surface, taking measurements over a melting ice surface is problematic (Smeets *et al.*, 1999). Profile z_0 is very sensitive to instrument height (Foken, 2008), with an offset of +0.1 m supposedly altering z_0 by an order of magnitude and doubling the estimated sensible heat flux (Munro, 1989). In micrometeorological studies, a height correction is sometimes applied to compensate for the breakdown of a log-linear wind

profile due to the influence of the forest canopy (Foken, 2008). This correction is based on the difference between 'actual' ground level and the height at which extrapolated wind speed drops to zero, which is usually somewhere near the top of the canopy. This principle has been adopted in glaciology to compensate for surface slope and variable topography, which can lead to the mean surface being beneath the apparent local surface of the glacier when considering the whole surface of the glacier (Munro, 1989; Sicart *et al.*, 2005), but defining a zero reference plane on a degrading or non-planar surface is challenging. Various workarounds have been suggested to mitigate the impact of an uneven, melting surface (e.g. Brock *et al.*, 2006; Sicart *et al.*, 2014; Fitzpatrick *et al.*, 2017; Quincey *et al.*, 2017), yet the most effective method remains unclear.

MO similarity theory assumes a homogeneous fetch (upwind area) is present (i.e. with consistent aerodynamic properties), but this is rarely found on glaciers (Brock *et al.*, 2006; Miles *et al.*, 2017; Quincey *et al.*, 2017). Moreover, it is unclear over what distance the fetch should be homogeneous, and several measurement height-fetch length ratios are proposed, including 1:100 (Wieringa, 1993) and 1:200 (Bradley, 1968). Recent EC work shows that 80% of flux contribution comes from within 150-200 m upwind of the measurement point when instruments are 2 m above the surface (Fitzpatrick *et al.*, 2019) – this suggests that a ratio of c.1:100 will incorporate the aerodynamically important fetch.

The sensitivities for profile z_0 discussed in this section are summarized in Table 1. In subsequent sections we present the analysis of those we found to have the most severe effects on z_0.

2.2 Microtopographic z_0

Aerodynamic roughness is a function of surface roughness, particularly in fully turbulent flow conditions (Elliott, 1958; Bandyopadhyay, 2006; Smith, 2014). Therefore, surface roughness metrics can be used to assess aerodynamic roughness. Their much simpler field data requirements make them a viable alternative that can better characterise the observed spatial and temporal variability in z_0 (Munro, 1989; MacKinnon *et al.*, 2004). Variations of the microtopographic method have been developed over a range of surfaces, based on empirical measurements of physical properties including grain size (Bagnold, 1941), average obstacle height (Sellers, 1965), plan area of roughness elements (Fryrear, 1965; Counihan, 1971) and surface roughness wavelength (Baechlin *et al.*, 1992; Banke and Smith, 2008). A recent study by Nield *et al.* (2013) showed that those including some height index exhibited the best relationship with aerodynamic roughness, yet all of the current, empirical approaches lack a grounding in physical theory. The most widely used approach within glacial studies is based on the work of Lettau (1969), who showed that

$$z_0 = 0.5h^* \left(\frac{s}{S_A}\right) \quad (3)$$

where h^* is the effective (average) obstacle height (m), s is the silhouette (exposed frontal area) of an average roughness element (m^2), S_A is area in the horizontal plane of the site of interest (m^2) and 0.5 represents an average drag coefficient (Kutzbach, 1961; Lettau, 1969).

Microtopographic z_0 values derived from (3) appear to agree with wind profile-derived z_0 to within +/- 25% (Lettau, 1969). The relation was based on empirical experiments wherein increasing/decreasing roughness was simulated by the systematic emplacement/removal of bushel baskets upwind of an anemometer mast erected on an ice lake (Kutzbach, 1961).

Parameters in (3) are obtained easily in such a controlled environment, but not over glaciers where individual roughness elements are not distinct. Munro (1989) devised an influential interpretation of (3) based on simplified horizontal microtopographic transects perpendicular to the prevailing wind direction, and populated by modelled roughness elements of equal spacing and dimension. Terms in (3) were re-defined in order to find z_0 for a transect of length X (m), where h^* (m) is given by twice the standard deviation ($2\sigma_d$) of elevations after the mean elevation has been set to zero. Thereafter

$$s = \frac{2\sigma_d X}{2f}, \tag{4}$$

where f is the number of groups of positive elevation values, and

$$S_A = \left(\frac{X}{f}\right)^2. \tag{5}$$

Thus,

$$z_0 = \frac{f}{X}(\sigma_d)^2. \tag{6}$$

Whether collected manually, using photogrammetry-based edge detection algorithms (Rees, 1998; Rees and Arnold, 2006; Fassnacht *et al.*, 2009) or extracted from 3D digital surface models (Irvine-Fynn *et al.*, 2014; Miles *et al.*, 2017), the transect method can be used to show variation in aerodynamic roughness across a glacier and throughout the melt season (Brock *et al.*, 2006), challenging the assumption made in most energy balance studies that z_0 is spatially and temporally homogeneous (e.g. Braun and Hock, 2004; Bravo *et al.*, 2017). The simplification of microtopography in (6) imposes several assumptions about the surface (Smith et al., 2016a): (i) that all roughness elements are equally spaced and have equal dimensions; (ii) that the silhouette of roughness features is the same under different wind directions; and (iii) that no shading of downwind elements is caused by those upwind.

Assumption (ii) becomes problematic when considering a wind-perpendicular transect, as glacial surfaces often host anisotropic roughness features (e.g. sastrugi, crevasses, supraglacial channels) that can be oriented parallel to the prevailing wind. Smith et al. (2016a) point out that in such cases exposed frontal area (and thus impact on flow) would appear much larger in a perpendicular transect than is realistic, resulting in erroneously high z_0. Additionally, streamlined features exhibit a small drag coefficient (Wieringa, 1993; Macdonald *et al.*, 1998), raising questions about whether Lettau's (1969) average of 0.5 is an overestimate for bare ice (Smith *et al.*, 2016a) or an underestimate for debris-covered ice (Quincey *et al.*, 2017). Lettau adopted the 0.5 value after the drag coefficient (C_d) of upturned >4 m^3 bushel baskets was given as 0.45 in experiments by Kutzbach (1961), who followed Schlichting's (1937) expression which is valid for regular arrays of geometrically similar roughness elements (Wooding *et al.*, 1973). This likely represents a simplification of the actual drag characteristics of glacier surfaces, where distinct, uniform roughness elements are rare.

A 2D, wind-perpendicular transect also fails to consider the shading and sheltering of adjacent roughness elements which may be up- or down-wind of the transect (assumption (iii), Fitzpatrick *et al.*, 2019). Sheltering effects are characterized by the ratio between the exposed frontal area and ground area, or roughness density (Wooding *et al.*, 1973; Raupach, 1992). Equation (3) holds where the roughness density is $\lesssim$0.3, but at higher densities the wakes caused by roughness elements interfere with each other, reducing z_0 as air flow starts to skim over the top of elements rather than between and around them (Macdonald et al., 1998; Smith, 2014). Alternatives to (3) and (5) account for obstacle density (Rounce *et al.*, 2015) and drag coefficient (Macdonald et al., 1998), but so far lack robust testing and independent validation.

3D methods have been proposed to address the shortcomings of the transect method, coincident with the proliferation of high-resolution survey techniques such as Structure from Motion photogrammetry (SfM) (Carrivick *et al.*, 2016; Smith *et al.*, 2016b) and terrestrial laser scanning (TLS) (Smith *et al.*, 2011; Fey and Wichmann, 2017).These methods allow rapid data acquisition over much larger areas and shorter timescales than is feasible with more traditional manual surveys. Recent studies have used digital elevation models (DEMs) constructed from SfM (Irvine-Fynn *et al.*, 2014; Rounce et al., 2015; Miles et al., 2017) or TLS (Nield et al., 2013) data, from which transects can be extracted as the grid rows and columns. Smith et al. (2016a) obtained terms for (3) from both DEMs and filtered point clouds, allowing the previous assumptions to be relaxed by accounting for the total exposed frontal area and giving a value for each cardinal wind direction.

The increasingly widespread use of SfM mandates that an assessment of the inherent uncertainties and how they relate to z_0 is carried out. Georeferencing provides an important control on the shape of the modelled surface and correctly recording the location and accuracy of ground control points (GCPs) is key. Interrogation of the bundle adjustment processing step (which minimises the overall residual error by tuning camera orientations and parameters, slightly adjusting 3D point coordinates) is made possible using a precision estimation workflow (James et al., 2017a), which allows the effects of SfM precision on z_0 estimates to be quantified.

Whether 2D or 3D methods are employed, the inclusion of an average height index imposes a spatial boundary (Smith, 2014), and as such the resulting z_0 value is dependent on the length of transect or the area of the plot (Rees and Arnold, 2006; Smith *et al.*, 2016*a*; Quincey *et al.*, 2017; Fitzpatrick *et al.*, 2019).Further dependence is placed on the resolution of the data, with coarser resolution data effectively representing a filtered fine-resolution dataset (Quincey et al., 2017); that is, for a given transect length, a surface which is sampled every 10 cm will appear smoother than one that is sampled every millimetre, artificially reducing z_0.

The scale and resolution of the data (and thus to some extent z_0) is informed somewhat qualitatively by the allocation of an upper and lower topographic partition scale for the surface in question, larger than which is deemed overall topography and smaller than which is indistinguishable from measurement noise (Smith, 2014). That is, the chosen scale of the study will dictate the survey technique used, which in turn can decide the resolution and impact the estimated z_0. The required scales of topography can be isolated for analysis by detrending, and transects are often detrended linearly, where the mean elevation is set to zero (Munro, 1989). With 3D data, the same effect is achieved by subtracting the fitted plane (Smith et al., 2016a).

This is a robust approach with smaller transects/plots; however, linear (and planar) detrending is susceptible to scale dependence (Miles et al., 2017). For larger plots/transects or more complex topography, other detrending methods may be more appropriate to remove overall trends, such as coarse-DEM removal, median filtering or splines (Miles et al., 2017; Quincey et al., 2017). These methods necessitate careful evaluation of the topographic partition scales, as slight adjustment of the scale over which detrending is applied can give quite different roughness values (Grohmann *et al.*, 2011)

As with profile z_0 (Table 1), in Table 2 we summarise microtopographic sensitivities. A severity rating is assigned based on our analysis. Those to which z_0 is most sensitive are presented in Section 4.2 and others in the Supporting Information.

3. Location, data and methods

3.1 Location

Data were collected between 8th and 19th July 2017, from two glaciers in the Tarfala Valley, Sweden (Fig. 2). The valley, located at 67°55'N and 18°35'E, has a Sub-Arctic climate with a mean annual temperature of around -3.3°C and an average of ~1000 mm of precipitation per year (Carrivick *et al.*, 2015). The frequent precipitation, winds and cloud cover (Hock *et al.*, 1999) produce turbulent fluxes which often contribute up to 50% of local glacier surface energy balances (Carrivick and Hock, 1998). The study glaciers, Storglaciären (Stor) and Sydöstra Kaskasatjäkkaglaciären (SK), are oriented (and flow) West-East and North-South respectively. Sites were visited on alternating days with the exception of day 7 (14th July), when poor weather precluded fieldwork. At SK in particular, the surface changed throughout the study from snow-covered, through slush to bare ice.

3.2 Data and methods

3.2.1 Aerodynamic profile z_0 measurements

Two wind towers were erected, one at Stor and the other at SK, with instruments at five levels (Stor: 0.35, 0.72, 1.27, 1.85 and 2.39 m, SK: 0.35, 0.69, 1.30, 1.80 and 2.43 m). On each tower, wind speed was recorded using five NRG #40 cup anemometers, wind direction with one NRG 200P wind vane and air temperature with five shielded and passively-ventilated TinyTag TGP-4017 sensors, each at one-minute intervals for a total of 10 days at SK and 4 days at Stor. Instrument heights were re-measured at each repeat visit. Data were recorded on Campbell CR1000s with a 12 V battery stored at the base of each tower, and are presented in full in Fig. S1. Raw one-minute interval data of each variable were averaged over periods of 10 and 15 minutes for processing.

The resulting profiles were used along with equation (2) to calculate z_0 for each 10 or 15 minute time step. In so doing, wind speed is regressed against log(z), and the extrapolated model is used to find z_0. The filters listed below were then applied, either retaining or rejecting those profiles where: the extrapolated model deviated more than an acceptable amount away from a log-linear profile, changes in temperature over time indicate conditions were not

stationary, and wind speeds were too low to be reliably recorded by our instruments. Profiles of wind speed and temperature were filtered in 3 stages:

1) relaxed filters: rejected poor log-linear profile fits (r^2<0.95) and low wind speeds (<1 m s^{-1}) whilst assuming stability is valid for MO theory;
2) standard filters (as used by Quincey *et al.*, 2017) again assume valid MO stability, applying a stricter r^2 filter (rejecting r^2<0.99), a minimum wind speed filter (<1 m s^{-1}) and a stationarity filter (which identifies when mean air temperature changed by >0.25 °C min^{-1});
3) finally, a stability correction based on MO similarity theory was applied as a third step, in addition to the standard filters. We found L using an iterative approach, in which any profiles which required more than 10 iterations to converge with MO theory (and were thus unlikely to converge at all) were discarded.

An estimate of the error attached to each z_0 value was obtained by first isolating the raw one-minute interval data that had contributed to successful profile fits when averaged over a 10 or 15 minute period. Each one minute profile was then used to find z_0. The mean z_0 of the one minute profiles from each 10 or 15 minute period was then compared to the z_0 value given by the original averaged profile, and the standard deviation was used as an estimate of error, as it represents the higher and lower bounds of possible z_0 values for each time period.

Each of the data filters were varied systematically, testing whether they should be made stricter or could be relaxed. Previous studies have shown that introducing additional filters greatly reduces the number of profiles obtained (Radić *et al.*, 2017), whereas we altered the filter thresholds themselves using a Monte Carlo approach, generating n = 1000 different threshold values for each filter. Next, we tested the effect of adding several height corrections to each measured instrument height, replicating previous efforts to compensate for glacier slope and topographic undulations (Munro, 1989; Sicart *et al.*, 2014).

3.2.2 Microtopographic z_0 estimates

On each visit and when weather conditions allowed, photogrammetric surveys of each site were carried out using both a Phantom 3 UAV with gimbal-stabilized digital camera, and a Panasonic DMC-TZ60 compact digital camera mounted on an 8 m inspection pole and operated remotely via a wireless connection (see Table S1 for further details). Sites were surveyed on alternate days, giving a total of five survey days for each, from which one for each site was selected used to produce a digital elevation model (Table S3 and S4) to compare with aerodynamic profile data collected during conditions favourable for MO similarity theory.

SfM data processing was carried out using Agisoft PhotoScan Professional Edition (version 1.4.0), following the procedure outlined by James *et al.* (2017b) with further point cloud processing in CloudCompare 2.10 (CloudCompare, 2018). Following recommendations in James *et al.* (2019), camera/image specifications and processing settings are included in S3, and Tables S1 and S2. SfM precision analysis was carried out using the Monte Carlo approach of James *et al.* (2017a), in which repeated bundle adjustments are carried out with pseudo-

random offsets applied to image observations. SfM and raster method precision were estimated from the Monte Carlo output using a bespoke Matlab tool called sfm_georef (James and Robson, 2012). The routine was adapted to generate a dense point cloud and interpolate a digital elevation model (DEM) for each iteration (n = 1000), from which an estimate of microtopographic z_0 error was obtained (see S4).

Microtopographic z_0 was calculated using the commonly applied Munro (1989) transect method (treating each row/column of a DEM as a separate transect), and the DEM method used by Smith *et al.* (2016a) and Quincey *et al.* (2017), with the difference that h^* was calculated from twice the standard deviation of elevations above the detrended plane rather than the mean elevation. As noted by Smith *et al*. (2016a) the choice of statistic is somewhat arbitrary; twice the standard deviation above the detrended plane was chosen as it provided the closest approximation of average roughness height as used by Lettau (1969).

Sensitivity tests depend on the perturbation of one property while all others stay constant. The standard elevation datasets were 10x10 m in extent, had a resolution of 0.005 m pixel^{-1}, and were detrended using 2D linear/3D planar detrending depending on the z_0 method in question. Initial comparisons were made between the aerodynamic profile and microtopographic methods using the standard datasets. We then looked first at the dependence of z_0 on scale (c.f. Rees and Arnold, 2006; Quincey *et al.*, 2017), varying the size of the plot/length of transect incrementally from 1 m to the maximum that would allow the plot to remain a square; 39 m in the case of Stor and 29 m for SK. To investigate the influence of DEM resolution, we gradually degraded the grid/transect resolution from 0.005 to 0.5 m per pixel. As a final step, the standard datasets were detrended using coarse-DEM removal, with moving mean window sizes varying from 0.5 to 5 m.

4. Results

4.1 Profile z_0

The number of fitted profiles giving z_0 values acceptable to MO theory was reduced by more than 97% in all cases of filtered data (Table 3). Most data were discarded by the r^2 filter, as few profiles adhered to the log-linear profile required for MO theory (see Fig. S2 for examples). Using stricter filters was found to decrease z_0 in all cases but one, where the standard filters were applied to the 10 minute averaged data on Stor, giving a higher mean z_0 (8.07 mm) than the relaxed filters (6.11 mm). Introducing the MO stability correction left even fewer profiles, but these were more in line with previously published z_0 from the same location (Hock and Holmgren, 1996). The same pattern is seen in the standard deviation of z_0, where in all cases but one the value is reduced by stricter filters, partly due to the exclusion of those profiles that do not meet the conditions of MO theory, and partly due to the smaller number of profiles included.

The reduction in data by both filtering and averaging is illustrated by Fig. 3, which shows z_0 plot against time. There was no obvious systematic change in z_0 over time, despite the gradual change in surface cover at SK (upglacier from the wind tower) from snow to bare ice. The error bars on each z_0 value, which come from the standard deviation of z_0 in each group of ten un-

averaged minute-interval profiles, are smaller for the tightly grouped lower values of z_0 than they are for the higher values, which are much more scattered. To discount other possible influences on the distribution of z_0, we tested the effects of wind direction and atmospheric stability, finding that the impact of both was small (see S1 and S2, Fig. S3 and S4).

To test the sensitivity of z_0 to filter thresholds, we first varied the r^2 filter between 0.9 and 1 (Fig. 4a and b), finding that relaxing the filter slightly (e.g. $r^2 = 0.95$) increased the number of profiles included by an order of magnitude at both glaciers and for both average time periods, also increasing z_0 (10 min: SK = 8.7 mm, Stor = 6.2 mm, 15 min: SK = 9.3 mm, Stor = 6.2 mm). Varying the maximum allowable change in temperature between 0 and 1°C min^{-1} made little difference to z_0, with changes of <5 mm at both sites (Fig. S5a & S5c), indicating that atmospheric conditions were largely stationary throughout the data collection period. Finally, allowing profiles with wind speeds slower than 1 m s^{-1} increased z_0 in both cases (Fig. S5b & S5d), but risked including data below the cup anemometer stall speed (0.7 m s^{-1}). Raising the minimum wind speed reduced the number of profiles and slightly reduced z_0 (by <5 mm).

In keeping with the findings of others (c.f. Munro, 1989; Sicart *et al.*, 2014), adding any height correction increased z_0 at both sites (Fig. 4c). 10 minute averaged z_0 from SK more than tripled from 6.7 mm to 22.5 mm when a 0.2 m height correction was added. Stability corrected z_0 at both glaciers increased by <3 mm in all cases. While the order of magnitude increase observed by Munro (1989) when a 0.1 m correction is added was not seen here, the trend was largely for greater height corrections to increase z_0 until profiles were modified to the extent that they were rejected by filtering. The exception was the Stor data filtered by standard filters, which actually reduced when a height correction of >0.05 m was applied, as the two profiles which caused the higher mean value were filtered out. Almost the same patterns were given by the 15 minute averaged data, although z_0 was generally lower (Fig. 4d). The increase seen in SK z_0 with the standard filters was more pronounced, with a quadrupling of z_0 from 5.5 mm to 20.1 mm.

4.2 Microtopographic z_0

Direct comparison between methods showed that at both sites, microtopographic z_0 closely matched profile values to within <3 mm (Fig. 5). Compared to values of 1.9 mm at Stor and 2 mm at SK derived from aerodynamic profiles, wind-perpendicular transects (see Fig. S6 for examples) produced a median z_0 of 4.6 mm (Stor) and 2.4 mm (SK), and raster-based z_0 values were 4.1 mm (Stor) and 2.1 mm (SK). The median value was chosen for transect z_0 for its robustness to the outliers in the substantial spread of values obtained. Other directional values given by the raster method fell within 0.5 mm of each other, suggesting the surfaces were isotropic over the length scales relevant for z_0 here; only z_0 for the prevailing wind direction is shown.

Roughness element height, or the height metric denoted by h^*, has previously been proposed as the greatest control on z_0 (Nield *et al.*, 2013). Our transect z_0 data bear this out (Table 4), although when each parameter of the raster method (for each raster used in subsequent scale tests–SK $n = 29$, Stor $n = 39$) was tested for a relationship with z_0, the maximum coefficient of

determination (between h^* and z_0) was quite low at both sites ($r^2 = 0.2$). Nonetheless, similar h^* values for the raster and transect methods have given similar z_0 values despite the large differences in s and S_A.

The mean 3D precision of SfM-derived DEMs was 7 mm at SK and 5.7 mm on Stor. This translated to a z_0 precision of ±0.052 mm (SK) and ±0.027 mm (Stor). SfM processing was therefore considered to be a negligible source of calculated z_0 variability (Fig. S7).

For gradually larger plots, raster z_0 on Stor varied from 1.04 to 3.44 mm, and transect z_0 from 1.70 to 9.17 mm (Fig. 6a and b). On SK, raster z_0 ranged between 1.5 and 7.1 mm, and transect z_0 between 1.1 and 5.6 mm. The relationship between z_0 and scale is as expected for SK (c.f. Miles *et al.*, 2017; Quincey *et al.*, 2017). Raster z_0 follows a clear trend with plot size, whereas transect z_0 shows some variation but increases overall – both demonstrate significant relationships (r^2>0.9, p<0.05). The relationship is less clear on Stor, with the raster z_0 increasing with plot size up to 13 m, then decreasing slightly but remaining at ~4.6 mm. Transect z_0 shows more variation, reaching a maximum of 8.4 mm at 18 m and staying around 6.6 mm at greater lengths, and indeed showing a large spread of values for any given plot size.

When DEM resolution was coarsened gradually from 0.005 to 0.5 m per pixel, the effect at both sites was for z_0 to decrease (Fig. 6c and d). At SK, raster z_0 decreased from 2.1 mm to 0.1 mm, and at Stor from 4.1 mm to 0.16 mm. Median transect z_0 decreased from 2.1 mm to 0.2 mm at SK and from 4.6 mm to 0.4 mm at Stor. A clear inflection is visible on both plots, potentially indicating a switch between form (>0.02 m pix^{-1}) and grain (<0.02 m pix^{-1}) roughness being represented in the topographic data. In this case the increased z_0 at finer resolution highlights the importance of finer scales of roughness elements.

z_0 was found to be influenced by the detrending method used (Table 5). The length over which original DEMs were smoothed to obtain a coarse DEM was varied from 0.5 – 5 m. Longer smoothing lengths (e.g. 5 m) left a greater area above the detrended mean, thus greater h^*, and greater overall silhouette area (s). While S_A was also increased for transect data, the number of upcrossings (f) decreased substantially. Even with a DEM size of just 10 m^2 the method and degree of detrending bears significant weight on the resulting z_0 value.

5. Discussion

5.1 Profile z_0

We employed the aerodynamic profile method to calculate z_0 over two glaciers during the 2017 ablation season, using the same experimental set up and methods as Quincey *et al.* (2017). After intensive field data collection z_0 was derived from profiles of wind speed and air temperature using MO similarity theory. Following the application of the MO stability correction, the profile z_0 values found for SK (1.7 - 2.0 mm) and Stor (2.4 – 2.5 mm) fall within the range that has been found previously for clean ice (i.e. not debris-covered) glaciers (see summary tables in Brock *et al.*, 2006; Miles *et al.*, 2017). In particular, the values for Storglaciären were very close to those used in an earlier study that used profiles at the same site (Hock and Holmgren, 1996). Without the stability correction, values fall within the upper end of the same range and overlap with those commonly found over debris-covered glaciers

(~10^1 mm) (Takeuchi *et al.*, 2000; Brock *et al.*, 2010; Quincey *et al.*, 2017). Applying the MO stability correction was found to reduce the scatter of z_0 values obtained, which is thought to be for a combination of two reasons: first, that only those profiles that most closely fit MO theory are retained, and second, that the number of profiles retained is greatly reduced.

Generally, site observations are reflected by the z_0 values obtained; Stor was visibly rougher than the site at SK, although a more pronounced progression of average daily z_0 values was expected at SK, where the fetch transitioned from snow, through slush, to bare ice during the data collection period. This is attributed to the study duration, where the site likely was not observed for long enough to allow detailed temporal analysis.

As with other similar studies, we found that using wind/temperature profiles to find z_0 is a very low-yield approach (c.f. Smeets *et al.*, 1998; Denby and Smeets, 2000; Brock *et al.*, 2006; Sicart *et al.*, 2014; Miles *et al.*, 2017; Quincey *et al.*, 2017). Moreover, sensors had to be monitored and repaired due to harsh weather conditions meaning that instruments cannot be set up and left unattended for long periods (the wind tower at Storglaciären collapsed overnight from 12th-13th July, hence the shortened dataset). Aggressive filtering of aerodynamic data left a small proportion of z_0 estimates remaining, 0.5% for SK and 0.6% for Stor (Fig. 3); this calls into question the ability of those few z_0 values to represent the roughness length adequately and echoes past criticisms of the suitability of MO stability theory for use over glaciers (Denby and Greuell, 2000; Denby and Smeets, 2000). By slightly relaxing the threshold used to filter out poor profile fits from $r^2 = 0.99$ to $r^2 = 0.95$, we were able to increase the number of profiles included by an order of magnitude while maintaining a similar z_0 and still only using statistically strong fits (Table 3), although z_0 was increased above the majority of published values for similar surfaces.

Past workers have attempted to account for local topographic variability so that z_0 measurements are made from the mean surface elevation rather than one point (e.g. Munro, 1989; Sicart *et al.*, 2014). Our testing corroborated past observations that adding a height correction increased z_0, although as shown by data from Storglaciären, the effect was not consistent (particularly with a limited dataset).

The inclusion of a stability correction, whether based on the Obukhov length L or the bulk Richardson number (Mölg *et al.*, 2008; Anderson *et al.*, 2010; Brock *et al.*, 2010; Radić *et al.*, 2017), has been questioned for its effect on the validity of MO similarity theory over glaciers, as both corrections have led to overestimations of the sensible-heat fluxes (Fitzpatrick *et al.*, 2017; Radić *et al.*, 2017). Here, the effect of including the MO stability correction was to drastically reduce the number of z_0 values produced (Fig. 3a and b), at the same time reducing z_0 to values similar to those obtained microtopographically (Fig. 5) and in other studies.

5.2 Microtopographic z_0

Estimates of z_0 were made using microtopographic data derived from SfM surveys of the two sites. Monte Carlo-based precision analysis (S4) showed that the impact of uncertainties within the bundle adjustment stage of the SfM workflow on microtopographic z_0 were minimal (two orders of magnitude smaller than z_0), offering confidence to this kind of data collection. A 'base case' was defined for microtopographic investigations at each site, where grid size was

kept at 10 x 10 m and DEM resolution was 0.005 m pixel^{-1}. The transect and raster methods were then used to estimate z_0 for comparison with profile values, using the median of all rows and columns for transect z_0 and the prevailing wind direction for raster z_0. Estimates for both methods compared well with profile measurements, to within <3 mm (Fig. 5), despite the large spread of values given by the transect method. Values also compare with those obtained over similar surfaces in other studies, where z_0 has been microtopographically estimated at ≤5 mm (Brock *et al.*, 2006; Smith, Quincey, *et al.*, 2016; Fitzpatrick *et al.*, 2018) While Nield *et al.* (2013) point out that the height metric exerts the greatest control over z_0 and offer some guidance for which metric might be more appropriate for different kinds of terrain, Smith *et al.* (2016a) point out that the rationale for twice the standard deviation of roughness elements is not explicit in Munro (1989). As the full range of elevations is sampled, not just the peak elevation of each obstacle (indeed the elevation field cannot really be disaggregated into a set of 'obstacles'), we chose to maintain the $2\sigma_d$ definition of h^* to preserve the influence of the larger roughness elements.

As with other studies of glacial z_0 (Rees and Arnold, 2006; Miles *et al.*, 2017; Quincey *et al.*, 2017), we found significant scale dependence within both microtopographic methods tested, which undermines the fact that values compare well to profile z_0. Generally, z_0 increased as it was estimated from larger grids and longer transects, suggesting that validation with independent methods (i.e. aerodynamic profiles) is the best way to decide on the appropriate scale. Similarly, z_0 decreased when calculated from coarser resolution elevation data (Fig. 6c and d), demonstrating the fractal properties of the surface (Arnold and Rees, 2004) and owing to the removal of finer-scale variability and an effectively smoother surface (Quincey *et al.*, 2017). Interestingly, Fitzpatrick *et al.* (2019) obtained values of $z_0 \approx 3$ mm over bare ice in British Columbia, Canada, using their block method (which finds z_0 for 1 m^2 cells based on the surrounding 9 m^2 moving window). Their values are comparable to those found here despite the smaller plot size (expected smaller z_0) and coarser resolution of 1 m pixel^{-1} (also expected smaller z_0). Despite the realistic values given by the microtopographic methods used here, their scale and resolution dependence are critical shortcomings that should be addressed as microtopographic methods develop. Fitzpatrick et al. (2019) also present a scale-independent transect method - this valuable progression has yet to be developed into a 3D method that can take full advantage of the scope of high-resolution survey techniques, and has yet to be tested glacier-wide.

Using a smaller plot size or coarser resolution elevation data has the benefit that detrending becomes a more straightforward task, as the influence of the overall slope becomes smaller (Smith, 2014). Table 5 demonstrates that the level of detrending can alter the character of the surface and thus z_0. Where smaller plots or shorter transects are used (e.g. <10 m) then linear/planar detrending is usually sufficient. Over scales >10 m the overall slope of the glacier surface can start to distort the detrended data, particularly on more convex surfaces like SK, necessitating other approaches. A possible solution to this is to calculate z_0 using a moving window (e.g. Fitzpatrick *et al.*, 2019), whereby z_0 is calculated for each cell based on adjacent cells within a specified radius (or window) - this way larger grids can still be used without the complication of deciding on the most appropriate detrending technique. This is more

computationally demanding than performing the detrending step once per plot and assumes that the resolution/scale dependence problem has been considered beforehand.

5.3 Future work

In order to ensure future attempts at parameterising z_0 microtopographically are validated correctly, the data against which they are validated must be reliable. Our test of relaxing the r^2 filter for aerodynamic profile fits should be tested with other datasets, so the yield from the method can be maximized. In the absence of eddy covariance equipment and data, we found the z_0 values obtained from wind profiles to be realistic compared to those in other similar studies (e.g. Brock *et al.*, 2006; Quincey *et al.*, 2017), and would suggest that the method be used with care, giving consideration to the sensitivities and uncertainties discussed here.

The characterisation of surface geometry should also be interrogated further, to ensure that the basis of the microtopographic approach is sound. The raster method improves upon the transect method by accounting for some of the effects of shading/sheltering (Smith et al., 2016a), yet the effects of wake interference between adjacent and successive roughness elements (Raupach, 1992) remains unaccounted for. The partition of drag between roughness elements and the underlying 'surface' (Raupach, 1992) will also depend on the upper and lower limits of topographic scale used to define a roughness element, considering the self-similar nature of glacier surfaces (Arnold and Rees, 2004).

Scale is another important area which should receive attention if 3D microtopographic methods are to be used to find glacier-wide distributed values of z_0. Here, a 10 x 10 m grid where each cell was 5 x 5 mm produced values very close to those obtained from aerodynamic profiles. In a scenario where glacier-wide microtopographic z_0 were being calculated using remotely sensed data, obtaining and processing data of the same resolution used here would be extremely computationally demanding. Moreover, as shown by this study, maintaining the same resolution and increasing scale would inflate z_0 estimates. Ideally, a scale independent 3D method would be used. Until this is developed, z_0 could potentially be reduced enough to balance the inflation by using a degraded resolution. If this can be calibrated correctly over a broad range of empirical data from different ice surfaces, then the feasibility of acquiring spatially and temporally distributed z_0 estimates from other readily available sources of remotely sensed data (i.e. satellites) could be explored.

6. Conclusions

We implemented the two most common methods for quantifying the aerodynamic roughness length (z_0) of glaciers, which are based on aerodynamic profiles or microtopographic data. Each has uncertainties and sensitivities which can ultimately impact the calculation of the contribution of the turbulent fluxes to the surface energy balance. Here, we provided a synthesis of these uncertainties and sensitivities, and presented an analysis of those we found to have the greatest impact on z_0. We conclude that:

1. While the eddy covariance method remains the standard for measuring flux and z_0, where such data are unavailable the profile and microtopographic methods can provide realistic z_0 values from equipment that is cheaper and more practical. The typical threshold for what constitutes an acceptable log-linear profile of air temperature or wind velocity can potentially

be relaxed slightly, e.g. from r2 = 0.99 to r2 = 0.95, increasing the number of included profiles, although this requires further investigation to ensure impact on z_0 is limited.

2. The transect and raster methods both produced estimates of z_0 comparable to values derived from aerodynamic profiles at the resolution and scale used in this study. The transect method produced a large spread of values, of which the average was close to profile z_0 yet some were an order of magnitude greater; the raster method, however, produced singular values which were extremely close to profile z_0. Both methods are susceptible to scale and resolution dependence, and the choice of detrending method. The choice of height metric (denoted by h*) is also important – uniform roughness elements can be represented by their mean height, yet this does not adequately approximate the surface where heights are uneven. Incorporating drag and sheltering effects could align the microtopographic approach more closely to its intended aerodynamic representation.

3. Calibrating the balance between scale and resolution of microtopographic data will be an important step in future work attempting to upscale the microtopographic approach to obtain glacier-wide estimates of z_0. This will enable us to test the feasibility of using broader scale (i.e. satellite) remotely sensed data as a means for obtaining spatially and temporally distributed z_0.

Acknowledgements

JRC is supported by a NERC PhD studentship (NE/L002574/1). Fieldwork was funded by an INTERACT transnational access grant awarded to MWS under the European Union H2020 Grant Agreement No.730938. The authors declare that they have no conflicts of interest. Data are currently being deposited and will be available by the date of publication from the UK Polar Data Centre, DOI to be provided.

References

Anderson, B., Mackintosh, A., Stumm, D., George, L., Kerr, T., Winter-Billington, A., and Fitzimons, S. (2010). Climate sensitivity of a high-precipitation glacier in New-Zealand. *J. Glaciol.* 56(195), 114-128(15).

Andreas, E. L., Persson, P. O. G., Grachev, A. A., Jordan, R. E., Horst, T. W., Guest, P. S., and Fairall, C. W. (2010). Parameterizing Turbulent Exchange over Sea Ice in Winter. *Journal of Hydrometeorology* 11(1), 87–104.

Arnold, N. S., and Rees, W. G. (2004). Self-similarity in glacier surface characteristics. *Journal of Glaciology* 49(167), 547–554.

Arnold, N. S., Rees, W. G., Hodson, A. J., and Kohler, J. (2006). Topographic controls on the surface energy balance of a high Arctic valley glacier. *Journal of Geophysical Research: Earth Surface* 111(2).

Baechlin, W., Theurer, W., and Plate, E. J. (1992). Dispersion of gases released near the ground in built up areas: Experimental results compared to simple numerical modelling. *Journal of Wind Engineering and Industrial Aerodynamics* 44(1–3), 2721–2732.

Bagnold, R. A. (1941). *The Physics of Blown Sand and Desert Dunes*. New York: Dover Publications Inc.

Bandyopadhyay, P. R. (2006). Rough-wall turbulent boundary layers in the transition regime. *Journal of Fluid Mechanics* 180(1), 231.

Banke, E. G., and Smith, S. D. (2008). Wind stress on Arctic sea ice. *Journal of Geophysical Research* 78(33), 7871–7883.

Bradley, E. F. (1968). A micrometeorological study of velocity profiles and surface drag in the region modified by a change in surface roughness. *Quarterly Journal of the Royal Meteorological Society* 94(401), 361–379.

Braun, M., and Hock, R. (2004). Spatially distributed surface energy balance and ablation modelling on the ice cap of King George Island (Antarctica). *Global and Planetary Change* 42(1–4), 45–58.

Bravo, C., Loriaux, T., Rivera, A., and Brock, B. W. (2017). Assessing glacier melt contribution to streamflow at Universidad Glacier, central Andes of Chile. *Hydrology and Earth System Sciences* 21(7), 3249–3266.

Brock, B. W., Mihalcea, C., Kirkbride, M. P., Diolaiuti, G., Cutler, M. E. J., and Smiraglia, C. (2010). Meteorology and surface energy fluxes in the 2005-2007 ablation seasons at the Miage debris-covered glacier, Mont Blanc Massif, Italian Alps. *Journal of Geophysical Research Atmospheres* 115(9), 1–16.

Brock, B. W., Willis, I. C., and Sharp, M. J. (2006). Measurement and parameterization of aerodynamic roughness length variations at Haut Glacier d'Arolla, Switzerland. *Journal of Glaciology* 52(177), 281–297.

Burba, G. (2013). *Eddy Covariance Method-for Scientific, Industrial, Agricultural, and Regulatory Applications*. Lincoln, Nebraska: LI-COR Biosciences doi:10.1007/s00704-004-0095-y.

Carrivick, J. L., and Hock, R. (1998). Measured and modelled melt and the surface energy

balance on Storglaciären. In Klingbjer, P. (Ed.), *Tarfala Research Station Annual Report, 1999*.

Carrivick, J. L., Smith, M. W., and Carrivick, D. M. (2015). Terrestrial laser scanning to deliver high-resolution topography of the upper Tarfala valley, arctic Sweden. *Gff* 137(4), 383–396.

Carrivick, J. L., Smith, M. W., and Quincey, D. J. (2016). *Structure from Motion in the Geosciences*. John Wiley & Sons.

Counihan, J. (1971). Wind Tunnel Determination of the Roughness Length As a Function of the Three-Dimensional Roughness Elements. *Atmospheric Environment* 5(1967), 637–642.

Denby, B. (1999). Second-Order Modelling of Turbulence in Katabatic Flows. *Boundary-Layer Meteorology* 92(1), 65–98.

Denby, B., and Greuell, W. (2000). The Use of Bulk and Profile Methods for Determining Surface Heat Fluxes in the Presence of Glacier Winds. *Journal of Glaciology* 46(154), 445–452.

Denby, B., and Smeets, C. J. P. P. (2000). Derivation of Turbulent Flux Profiles and Roughness Lengths from Katabatic Flow Dynamics. *Journal of Applied Meteorology* 39(9), 1601–1612.

Dyer, A. J., and Hicks, B. B. (1970). Flux-gradient relationships in the constant flux layer. *Quarterly Journal of the Royal Meteorological Society* 96(410), 715–721.

Elliott, W. P. (1958). The growth of the atmospheric internal boundary layer. *Eos, Transactions American Geophysical Union* 39(6), 1048–1054.

Fassnacht, S. R., Stednick, J. D., Deems, J. S., and Corrao, M. V. (2009). Metrics for assessing snow surface roughness from Digital imagery. *Water Resources Research* 46(4).

Fausto, R. S., Van As, D., Box, J. E., Colgan, W., Langen, P. L., and Mottram, R. H. (2016). The implication of nonradiative energy fluxes dominating Greenland ice sheet exceptional ablation area surface melt in 2012. *Geophysical Research Letters* 43(6), 2649–2658.

Favier, V., Wagnon, P., Chazarin, J. P., Maisincho, L., and Coudrain, A. (2004). One-year measurements of surface heat budget on the ablation zone of Antizana Glacier 15, Ecuadorian Andes. *Journal of Geophysical Research Atmospheres* 109(18), 1–15.

Fey, C., and Wichmann, V. (2017). Long-range terrestrial laser scanning for geomorphological change detection in alpine terrain – handling uncertainties. *Earth Surface Processes and Landforms* 42(5), 789–802.

Fitzpatrick, N., Radić, V., and Menounos, B. (2019). A multi-season investigation of glacier surface roughness lengths through in situ and remote observation. *The Cryosphere* 13, 1051–1071.

Fitzpatrick, N., Radic, V., and Menounos, B. (2018). A multi-season investigation of glacier surface roughness lengths through in situ and remote observation. *The Cryosphere Discussions* (November), 1–39. doi:10.5194/tc-2018-232.

Fitzpatrick, N., Radić, V., and Menounos, B. (2017). Surface Energy Balance Closure and Turbulent Flux Parameterization on a Mid-Latitude Mountain Glacier, Purcell Mountains, Canada. *Frontiers in Earth Science* 5(September), 1–20.

Foken, T. (2006). 50 years of the Monin-Obukhov similarity theory. *Boundary-Layer Meteorology* 119(3), 431–447.

Foken, T. (2008). *Micrometeorology*. Berlin: Springer.

Fryrear, D. W. (1965). Soil cover and wind erosion. *Transactions of the ASAE* 28(3), 781–784.

Garratt, J. R. (1992). *The Atmospheric Boundary Layer*. Cambridge: Cambridge University Press.

Giesen, R. H., Andreassen, L. M., Oerlemans, J., and Van Den Broeke, M. R. (2014). Surface energy balance in the ablation zone of Langfjordjøkelen, an arctic, maritime glacier in northern Norway. *Journal of Glaciology* 60(219), 57–70.

Gorter, W., van Angelen, J. H., Lenaerts, J. T. M., and van den Broeke, M. R. (2014). Present and future near-surface wind climate of Greenland from high resolution regional climate modelling. *Climate Dynamics* 42(5–6), 1595–1611.

Greuell, W., and Genthon, C. (2004). Modelling land-ice surface mass balance. In *Mass Balance of the Cryosphere*. doi:10.1017/CBO9780511535659.007.

Grohmann, C. H., Smith, M. J., and Riccomini, C. (2011). Multiscale analysis of topographic surface roughness in the Midland Valley, Scotland. *IEEE Transactions on Geoscience and Remote Sensing*. doi:10.1109/TGRS.2010.2053546.

Hock, R. (2005). Glacier melt: a review of processes and their modelling. *Progress in Physical Geography* 29(3), 362–391.

Hock, R., Carrivick, J. L., and Jonsell, U. (1999). Glacio-meteorological studies on Storglaciären in 1999. In *Tarfala Research Station Annual Report, 1999*.

Hock, R., and Holmgren, B. (1996). Some Aspects of Energy Balance and Ablation of Storglaciären , Northern Sweden. *Geografiska Annaler Series A-Physical Geography* 78(2), 121–131.

Inoue, J., and Yoshida, M. (1980). Ablation and Heat Exchange over the Khumbu Glacier. *Journal of the Japanese Society of Snow and Ice* 41(Special), 26–33.

Irvine-Fynn, T. D. L., Sanz-Ablanedo, E., Rutter, N., Smith, M. W., and Chandler, J. H. (2014). Measuring glacier surface roughness using plot-scale, close-range digital photogrammetry. *Journal of Glaciology* 60(223), 957–969.

James, M.R., Chandler, J. H., Eltner, A., Fraser, C., Miller, P. E., Mills, J. P., Noble, T., Robson, S., and Lane, S. N. (2019). Guidelines on the use of Structure from Motion Photogrammetry in Geomorphic Research. *Earth Surface Processes and Landforms*. doi:10.1002/esp.4637.

James, Mike R., and Robson, S. (2012). Straightforward reconstruction of 3D surfaces and topography with a camera: Accuracy and geoscience application. *Journal of Geophysical Research: Earth Surface* 117(F03017).

James, Mike R., Robson, S., D'Oleire-Oltmanns, S., and Niethammer, U. (2017). Optimising

UAV topographic surveys processed with structure-from-motion: Ground control quality, quantity and bundle adjustment. *Geomorphology* 280, 51–66.

James, Mike R., Robson, S., and Smith, M. W. (2017). 3-D uncertainty-based topographic change detection with structure-from-motion photogrammetry: Precision maps for ground control and directly georeferenced surveys. *Earth Surface Processes and Landforms* 42, 1769–1788.

Lettau, H. (1969). Note on Aerodynamic Roughness-Parameter Estimation on the Basis of Roughness-Element Description. *J. Appl. Meteor.* 8(5), 828–832.

Litt, M., Sicart, J. E., Helgason, W. D., and Wagnon, P. (2014). Turbulence Characteristics in the Atmospheric Surface Layer for Different Wind Regimes over the Tropical Zongo Glacier (Bolivia, 16∘S). *Boundary-Layer Meteorology* 154(3), 471–495.

Litt, M., Sicart, J. E., Six, D., Wagnon, P., and Helgason, W. D. (2017). Surface-layer turbulence, energy balance and links to atmospheric circulations over a mountain glacier in the French Alps. *Cryosphere* 11(2), 971–987.

Macdonald, R. W., Griffiths, R. F., and Hall, D. J. (1998). An improved method for the estimation of surface roughness of obstacle arrays. *Atmospheric Environment* 32(11), 1857–1864.

MacKinnon, D. J., Clow, G. D., Tigges, R. K., Reynolds, R. L., and Chavez, P. S. (2004). Comparison of aerodynamically and model-derived roughness lengths (zo) over diverse surfaces, central Mojave Desert, California, USA. *Geomorphology* 63(1–2), 103–113.

Miles, E. S., Steiner, J. F., and Brun, F. (2017). Highly variable aerodynamic roughness length (z 0) for a hummocky debris-covered glacier. *Journal of Geophysical Research: Atmospheres* 122(16), 8447–8466.

Mölg, T., Cullen, N. J., Hardy, D. R., Kaser, G., and Klok, L. (2008). Mass balance of a slope glacier on Kilimanjaro and its sensitivity to climate. *International Journal of Climatology* 28, 881–892.

Monin, A. S., and Obukhov, A. M. (1954). Basic Laws of Turbulent Mixing in the Ground Layer of the Atmosphere. *Trans. Geophys. Inst. Akad. Nauk. USSR* 24(151), 163–187.

Munro, D. S. (1989). Surface roughness and bulk heat transfer on a glacier: comparison with eddy correlation. *Journal of Glaciology* 35(121), 343–348.

Nield, J. M., King, J., Wiggs, G. F. S., Leyland, J., Bryant, R. G., Chiverrell, R. C., Darby, S. E., Eckardt, F. D., Thomas, D. S. G., Vircavs, L. H., and Washington, R. (2013). Estimating aerodynamic roughness over complex surface terrain. *Journal of Geophysical Research Atmospheres* 118(23), 12948–12961.

Pelletier, J. D., and Field, J. P. (2016). Predicting the roughness length of turbulent flows over landscapes with multi-scale microtopography. *Earth Surface Dynamics* 4(2), 391–405.

Quincey, D. J., Smith, M. W., Rounce, D. R., Ross, A. N., King, O., and Watson, C. S. (2017). Evaluating morphological estimates of the aerodynamic roughness of debris covered glacier ice. *Earth Surface Processes and Landforms*. doi:10.1002/esp.4198.

Radić, V., Menounos, B., Shea, J., Fitzpatrick, N., Tessema, M. A., and Déry, S. J. (2017). Evaluation of different methods to model near-surface turbulent fluxes for an alpine

glacier in the Cariboo Mountains, BC, Canada. *The Cryosphere Discussions* , 1–39. doi:10.5194/tc-2017-80.

Raupach, M. R. (1992). Drag and drag partition on rough surfaces. *Boundary-Layer Meteorology* 60(4), 375–395.

Rees, W. G. (1998). A rapid method of measuring snow-surface profiles. *Journal of Glaciology* 44(c), 674–675.

Rees, W. G., and Arnold, N. S. (2006). Scale-dependent roughness of a glacier surface: Implications for radar backscatter and aerodynamic roughness modelling. *Journal of Glaciology* 52(177), 214–222.

Rounce, D. R., Quincey, D. J., and McKinney, D. C. (2015). Debris-covered glacier energy balance model for Imja-Lhotse Shar Glacier in the Everest region of Nepal. *Cryosphere* 9(6), 2295–2310.

Schlichting, H. (1937). Experimental investigation of the problem of surface roughness. *National Advisory Committee for Aeronautics: Technical Memorandum*.

Sellers, W. D. (1965). *Physical Climatology*. Chicago: University of Chicago Press.

Sicart, J. E., Litt, M., Helgason, W., Tahar, V. Ben, and Chaperon, T. (2014). A study of the atmospheric surface layer and roughness lengths on the high-altitude tropical Zongo glacier, Bolivia. *Journal of Geophysical Research* 119(7), 3793–3808.

Sicart, J. E., Wagnon, P., and Ribstein, P. (2005). Atmospheric controls of the heat balance of Zongo Glacier (16°S, Bolivia). *Journal of Geophysical Research D: Atmospheres* 110(12), 1–17.

Smeets, C. J. P. P., Duynkerke, P. G., and Vugts, H. F. (1998). Turbulence characteristics of the stable boundary layer over a mid-latitude glacier. Part I: a combination of katabatic and large-scale forcing. *Boundary-Layer Meteorology* 87(1), 117–145.

Smeets, C. J. P. P., Duynkerke, P. G., and Vugts, H. F. (1999). Observed wind profiles and turbulent fluxes over an ice surface with changing surface roughness. *Boundary-Layer Meteorology* 92(1994), 101–123.

Smith, M. W. (2014). Roughness in the Earth Sciences. *Earth-Science Reviews*.

Smith, M. W., Carrivick, J. L., and Quincey, D. J. (2016b). Structure from motion photogrammetry in physical geography. *Progress in Physical Geography* 40(2), 247–275.

Smith, M. W., Cox, N. J., and Bracken, L. J. (2011). Terrestrial laser scanning soil surfaces: A field methodology to examine soil surface roughness and overland flow hydraulics. *Hydrological Processes* 25(6), 842–860.

Smith, M. W., Quincey, D. J., Dixon, T., Bingham, R. G., Carrivick, J. L., Irvine-Fynn, T. D. L., and Rippin, D. M. (2016a). Aerodynamic roughness of glacial ice surfaces derived from high-resolution topographic data. *Journal of Geophysical Research F: Earth Surface* 121(4), 748–766.

Stiperski, I., and Rotach, M. W. (2016). On the Measurement of Turbulence Over Complex Mountainous Terrain. *Boundary-Layer Meteorology* 159(1), 97–121.

Stull, R. (1988). *An Introduction to Boundary Layer Meteorology*. Dordrecht: Kluwer.

Takeuchi, Y., Kayastha, R. B., and Nakawo, M. (2000). Characteristics of ablation and heat balance in debris-free and debris-covered areas on Khumbu Glacier, Nepal Himalayas, in the pre-monsoon season. *IAHS Publication* 264(2), 53–61.

Vavrus, S. J. (2013). Extreme Arctic cyclones in CMIP5 historical simulations. *Geophysical Research Letters* 40(23), 6208–6212.

Wieringa, J. (1993). Representative roughness parameters for homogeneous terrain. *Boundary-Layer Meteorology* 63(4), 323–363.

Wooding, R. A., Bradley, E. F., and Marshall, J. K. (1973). Drag due to regular arrays of roughness elements of varying geometry. *Boundary-Layer Meteorology* 5(3), 285–308.

Table 1 Sensitivities and uncertainties in finding glacier z_0 from aerodynamic profiles

Sensitivity	Description	Stage	Reference	Section	Severity*
Instrument height/reference level	Accounts for surface slope/topographic undulations. Can be dynamic as glacier surfaces evolve and equipment melts into the ice. Important for identifying shallow katabatic conditions.	Field/processing	Munro (1989) Garratt (1992) Foken (2008) Sicart *et al.* (2014)	**4.1** **Fig. 3c**	**High**
Stability correction	Used in near-neutral conditions commonly found over glaciers. Based on Monin-Obukhov similarity theory. Not applicable in strongly or weakly stable conditions. Reduces number of profiles which can be fitted and number of results, but important over ice where temperature gradients are strong.	Processing	Foken (2008) Radić *et al.* (2017) Fitzpatrick *et al.* (2018)	**4.1** **Fig. 3a and b**	**High**
Data filters (wind speed, stationarity, profile fitting)	Thresholds used to filter out data close to anemometer stall speed, non-stationarity and non-convergence of wind speed/temperature profiles. Can lead to majority of data being discarded.	Processing	Miles *et al.* (2017) Quincey *et al.* (2017) Radić *et al.* (2017)	**4.1** **Fig. 3d**	**Medium**
Time averaging	Period over which meteorological data are averaged. Can be applied before or after profile fitting, but reduces the quantity of profiles and can mask temporal trends.	Processing	Anderson *et al.* (2010) Cullen *et al.* (2007) Fitzpatrick *et al.* (2017)	**4.1**	**Medium**
Fetch/footprint	Wind speed at increasing measurement levels affected by obstacles at increasing distance from instruments. Homogeneous fetch desirable. Height/fetch ratio recommendations vary.	Field	Garratt (1992) Wieringa (1993) Foken (2008) Fitzpatrick *et al.* (2019)		**Medium**
Regression	In addition to filtering out weaker profile fits, stricter r^2 values can decrease the statistical error introduced by assigning variables incorrectly, i.e. measurement height as the dependent variable, and wind speed as the dependent variable.	Processing	Bauer *et al.* (1992)		**Medium**
Surface slope	Partly causes katabatic winds. On steeper slopes it is difficult to identify vertical/horizontal movement of air using cup anemometers.	Field/processing	Denby and Greuell (2000) Denby and Smeets (2000) Radić *et al.* (2017)		**Low**

*as suggested by the effect of each sensitivity on z_0 in this study

Table 2 Sensitivities and uncertainties in using microtopographic methods to find glacier z_0

Sensitivity	Description	Stage	Reference	Section	Severity*
Detrending	Appropriate detrending method depends on the scale of study – linear/planar is fine for smaller scales, but not for larger plots.	Processing	Quincey *et al.* (2017)	4.2 Table 5	**High**
Scale dependence	Longer transects/larger plots cause z_0 to increase.	Field/processing	Miles *et al.* (2017) Quincey *et al.* (2017) Rees & Arnold (2006)	4.2 Fig. 6a and b	**High**
Resolution dependence	Coarser resolution data causes z_0 to decrease.	Field/processing	Miles *et al.* (2017) Quincey *et al.* (2017) Rees & Arnold (2006)	4.2 Fig. 6c and d	**High**
Drag coefficient	0.5 is used as the "average". Depends on scale and density of roughness elements, surface anisotropy and wind direction, usually two orders of magnitude smaller for ice surfaces.	Field/processing	Munro (1975) Munro (1989) Quincey *et al.* (2017)		**Medium**
Assumptions of Munro (1989) equation	Simplification of Lettau (1969) equation used with transects assumes uniform spacing/height of roughness elements, no sheltering effects, and that z_0 is not reliant on wind direction.	Processing	Smith *et al.* (2016)		**Medium**
Disruption of surface	Field methods can alter the natural glacier surface, e.g. laying down a pole for a transect, placing GCPs for SfM surveys or walking with crampons.	Field	Brock *et al.* (2006)		**Low**
SfM/TLS uncertainties	Field uncertainties can be mitigated with robust survey design. Also worth considering doming effect, bundle adjustment and ground control.	Field/processing	James *et al.* (2017a)	4.2 Fig. S7	**Low**

*as suggested by the effect of each sensitivity on z_0 in this study

Table 3 Summary of effect of original and alternative filters on number of profiles and z_0 value. The unfiltered number of profiles is included in parentheses next to the site name. Standard deviation of z_0 is given along with mean z_0 values for each level of filtering and each averaging period. No standard deviation is given for stability corrected z_0 on Stor as only one value for z_0 was produced.

	SK (n = 10130)		**% of original**		**z_0 (mm)**		**Stor (n = 5682)**		**% of original**		**z_0 (mm)**	
	10	**15**	**10**	**15**	**10**	**15**	**10**	**15**	**10**	**15**	**10**	**15**
Relaxed filters	306	204	3%	2%	8.9 (±13.5)	9.4 (±14.3)	168	118	2.9%	2.1%	6.3 (±7.6)	6.3 (±6.7)
Standard filters	70	45	0.7%	0.44%	6.8 (±9.9)	5.5 (±9.3)	7	3	1.2%	0.05%	20.9 (±22)	6.7 (±3.3)
Stability corrected	6	4	0.06%	0.04%	2.0 (±0.63)	1.7 (±0.3)	1	1	0.02%	0.02%	2.4 (±0)	2.5 (±0)

Table 4 Summary of Lettau (1969) equation terms for raster and transect methods at both study sites. The values for the prevailing wind direction are given in each case, and transect values are the median of all rows/columns perpendicular to the prevailing wind. Note that s and S_A are included for information only, they represent very different areas for each method and are not comparable. Estimates of error for the raster method are taken from the standard deviation of values given by precision analysis (see S4). Those for the transect method are the standard deviation of all values produced.

	SK				Stor			
	z_0 (mm)	h^* (m)	s (m^2)	S_A (m^2)	z_0 (mm)	h^* (m)	s (m^2)	S_A (m^2)
Raster	2.4 (±0.05)	0.04	12.6	100.00	4.1 (±0.03)	0.06	14.3	100.00
Transect	2.1(±0.9)	0.05(±0.01)	0.008(±0.01)	0.1(±0.2)	4.6(±3.5)	0.1(±0.02)	0.02(±0.02)	0.16(±0.6)

Table 5 Summary of detrending method effects on z_0 and terms of Lettau (1969) equation. Values along the top row in metres refer to the length of window used to smooth original data. f refers to the number of upcrossings used in the Munro (1989) equation.

		SK					Stor				
		Planar/linear	5 m	2 m	1 m	0.5 m	Planar/linear	5 m	2 m	1 m	0.5 m
DEM	z_0 (mm)	1.7	11	3.1	1.2	0.4	3.1	3.2	1.9	1.4	0.9
	h* (m)	0.03	0.2	0.06	0.03	0.01	0.04	0.05	0.03	0.03	0.02
	s (m^2)	12.6	10.6	9.9	9.2	7.5	14.3	12.4	11.9	11.6	10.8
	S_A (m^2)	100	100	100	100	100	100	100	100	100	100
Transect	z_0 (mm)	2.1(±0.9)	1.5(±0.3)	1.6(±0.7)	1.2(±0.9)	0.7(±0.9)	4.6(±3.5)	5.2(±1.4)	3.1(±2.6)	2.5(±3.5)	1.6(±3.5)
	h* (m)	0.05(±0.01)	0.05(±0.01)	0.04(±0.7)	0.02(±0.01)	0.01(±0.01)	0.1(±0.02)	0.1(±0.02)	0.06(±0.02)	0.04(±0.02)	0.03(±0.9)
	s (m^2)	0.01(±0.01)	0.01(±0.01)	0.004(±0.01)	0.001(±0.01)	0.0004(±0.01)	0.03(±0.02)	0.02(±0.03)	0.007(±0.03)	0.003(±0.02)	0.001(±0.02)
	S_A (m^2)	0.15(±0.2)	0.1(±0.9)	0.04(±0.4)	0.01(±0.2)	0.004(±0.2)	0.40(±0.6)	0.2(±1.6)	0.06(±0.8)	0.03(±0.6)	0.01(±0.6)
	f	31(±11)	26(±4)	51(±8)	90(±11)	168(±11)	25(±13)	23(±5)	42(±9)	63(±13)	101(±13)

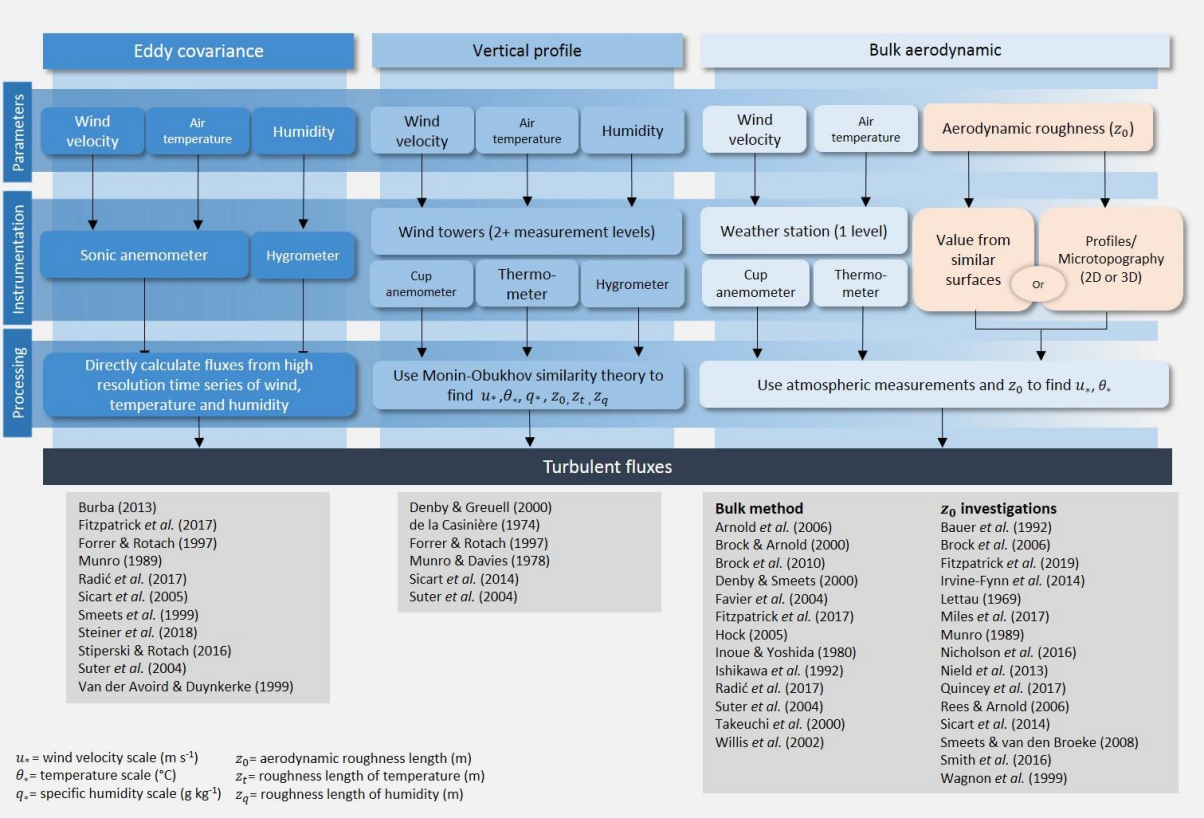

Fig. 1 Summary of techniques used to calculate turbulent fluxes. This research is concerned primarily with the right-hand portion of the figure (orange), where different methods can be used to obtain a value of z_0 for the bulk aerodynamic approach.

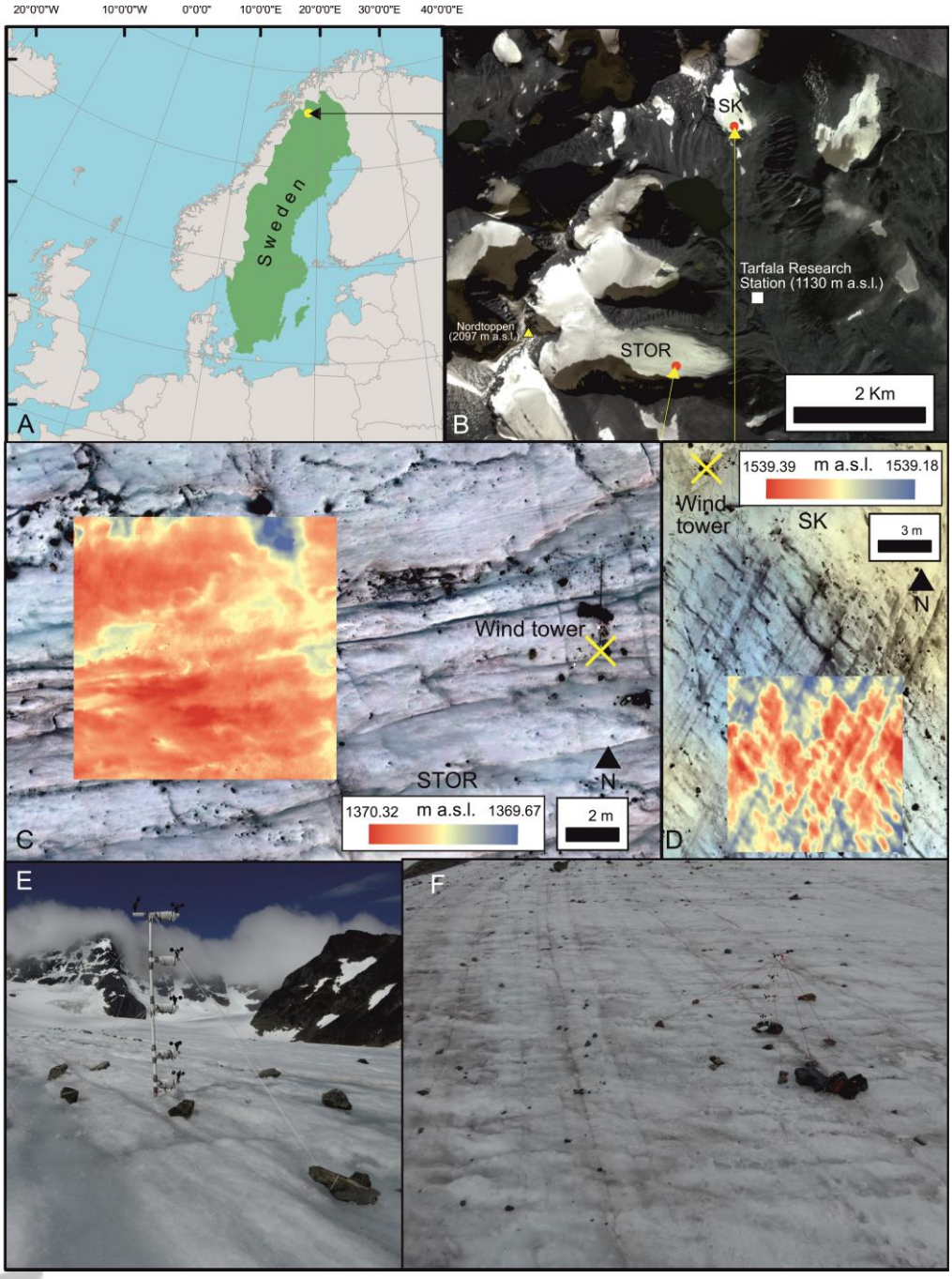

Fig. 2 Location of study in Tarfala Valley, Sweden (A). Satellite imagery (B) courtesy of Planet Labs (Planet Team, 2018). Lowermost images show location of wind towers on Stor (C) and SK (D), orthophotos were generated from SfM data for each site. Elevation overlays show the 10x10 m DEMs used as the base case for analysis of each site. (E) and (F) show the site around the wind towers at Stor (E) and SK (F). Both are looking roughly up-glacier.

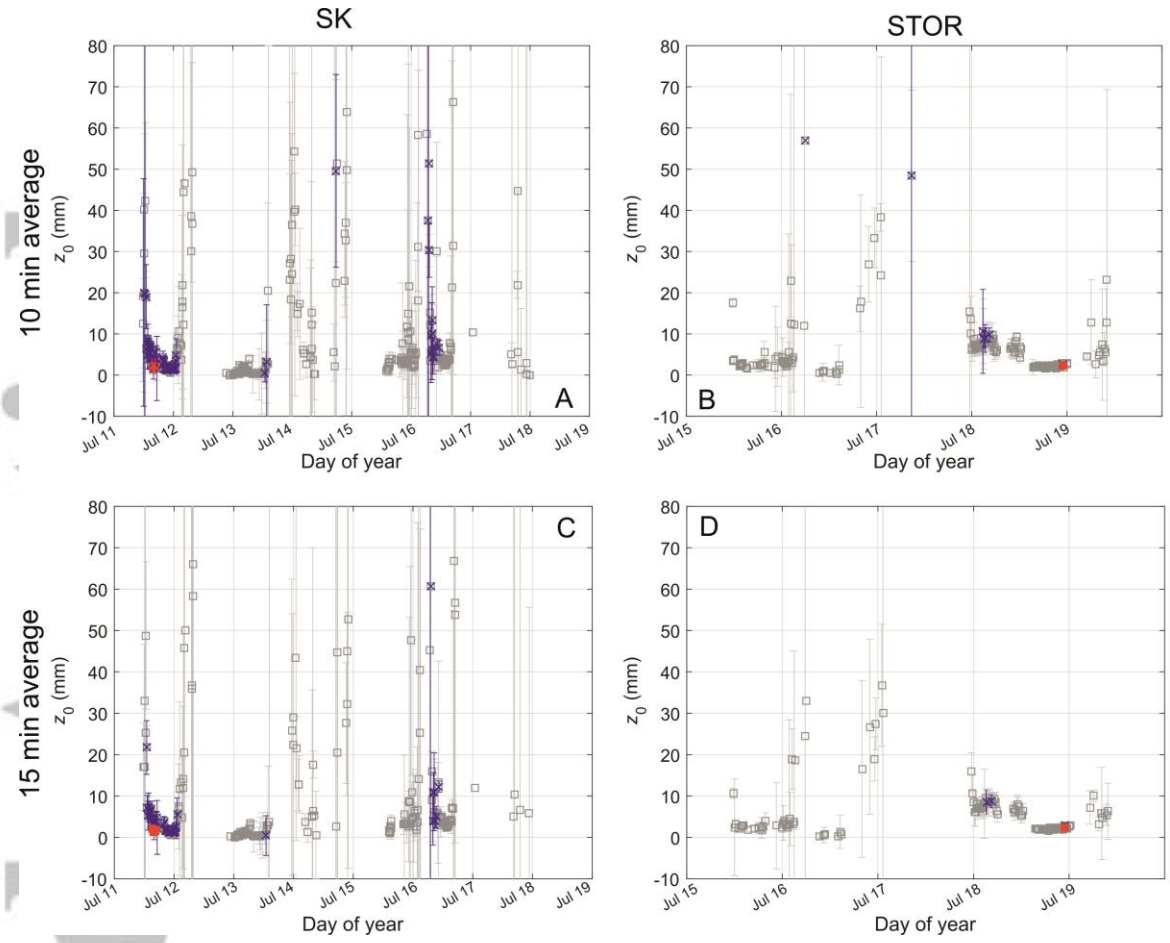

Fig. 3 Results of analysis of profile z_0 over time. Data from SK is shown in the left column, and Stor in the right. Results from input data which has been averaged over 10 minutes is shown in the top row, over 15 minutes in the bottom row. Data filtered using a relaxed filter are shown in grey, blue data points have been filtered with standard filters and red points show those to which the MO stability correction has been applied. Error bars are calculated from the standard deviation of z_0 from profiles of each minute that comprises each averaged block of data (i.e. ten profiles where data are averaged over ten minutes). Some error bars extend beyond the axis range used here.

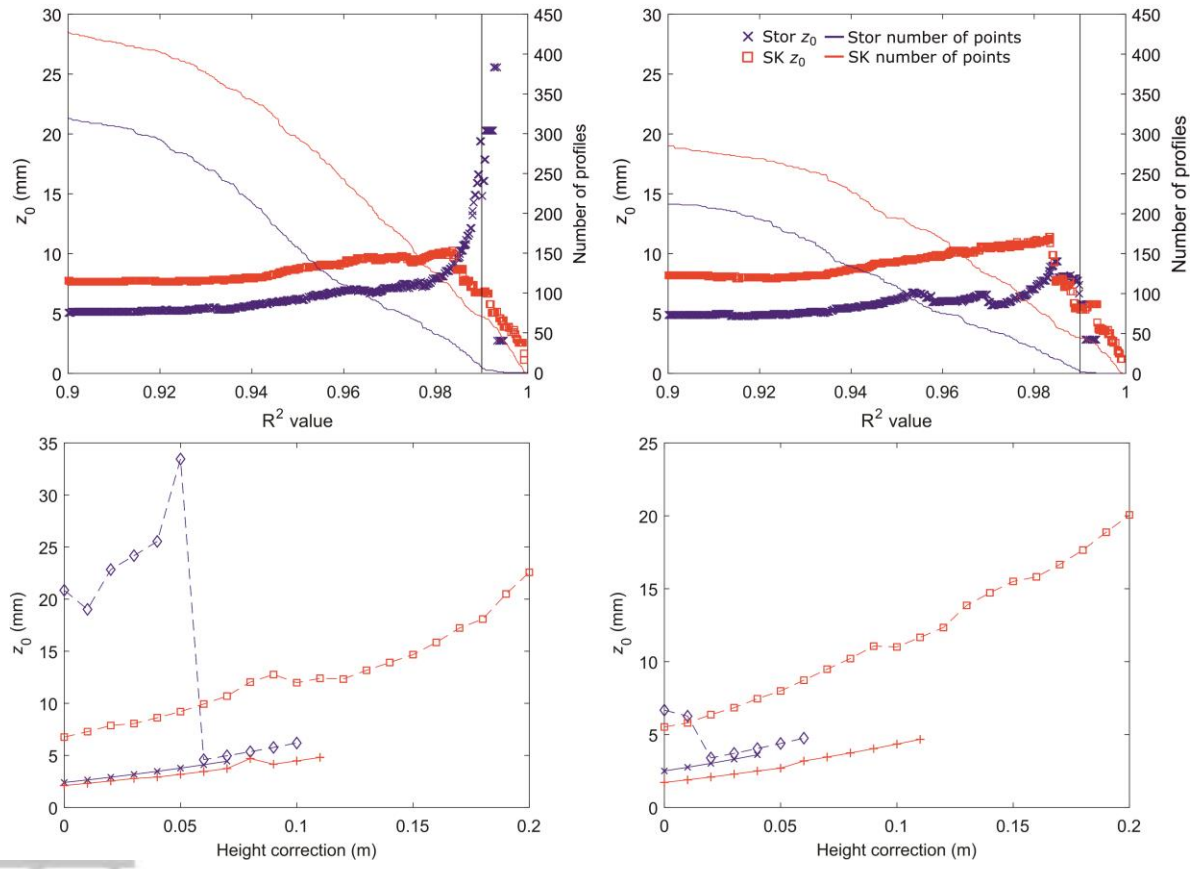

Fig. 4 Effect on z_0 of altering the r2 filter for 10 minute (a) and 15 minute (b) averaging times. A vertical line illustrates the 0.99 threshold normally used. Effects of adding a height correction are shown for averaging periods of 10 minutes (C) and 15 minutes (D).

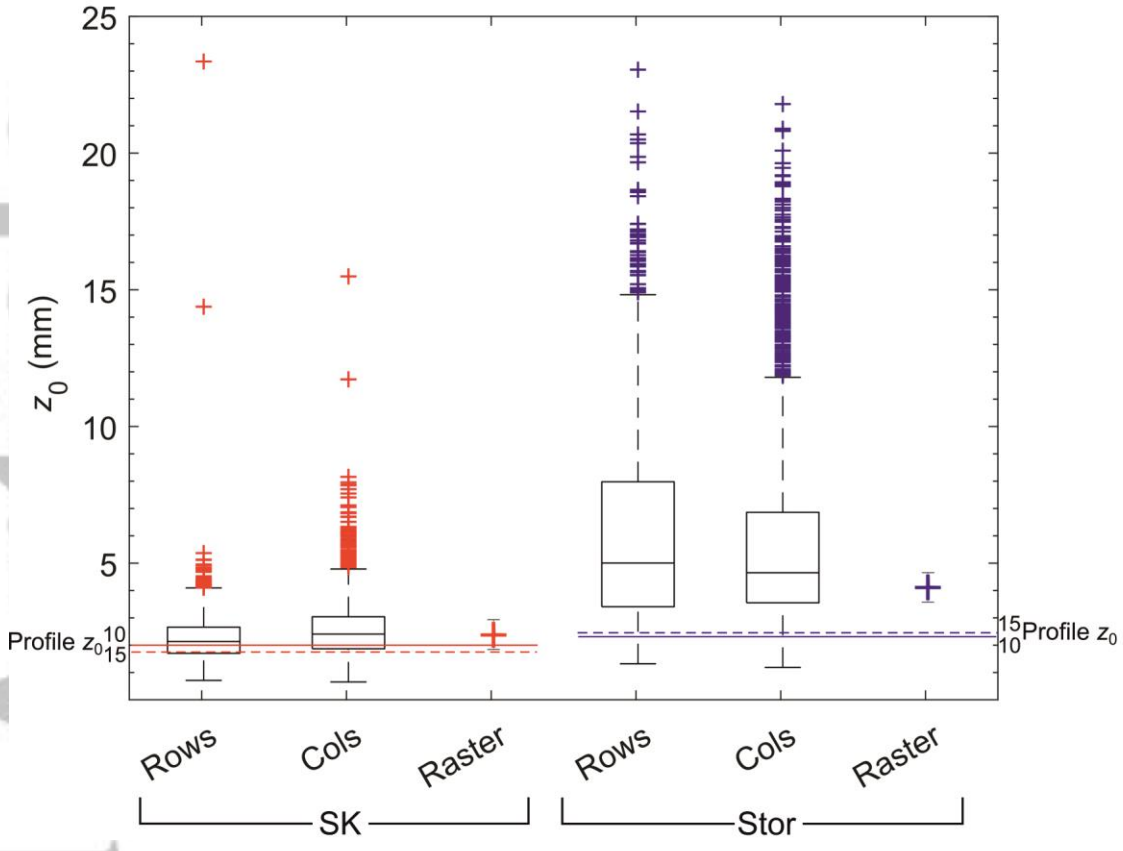

Fig. 5 Comparison of z_0 obtained from rasters, transects and stability corrected aerodynamic profiles. Due to the orientation of the glaciers, columns were wind-perpendicular on Stor, as were rows on SK. Colours of raster z_0 markers are coordinated with the profile z_0 reference lines (labelled). Profile z_0 given for 10 (solid lines) and 15 (dashed line) minute averaging periods, including stability are also shown, with error bars indicating the values given by precision analysis.

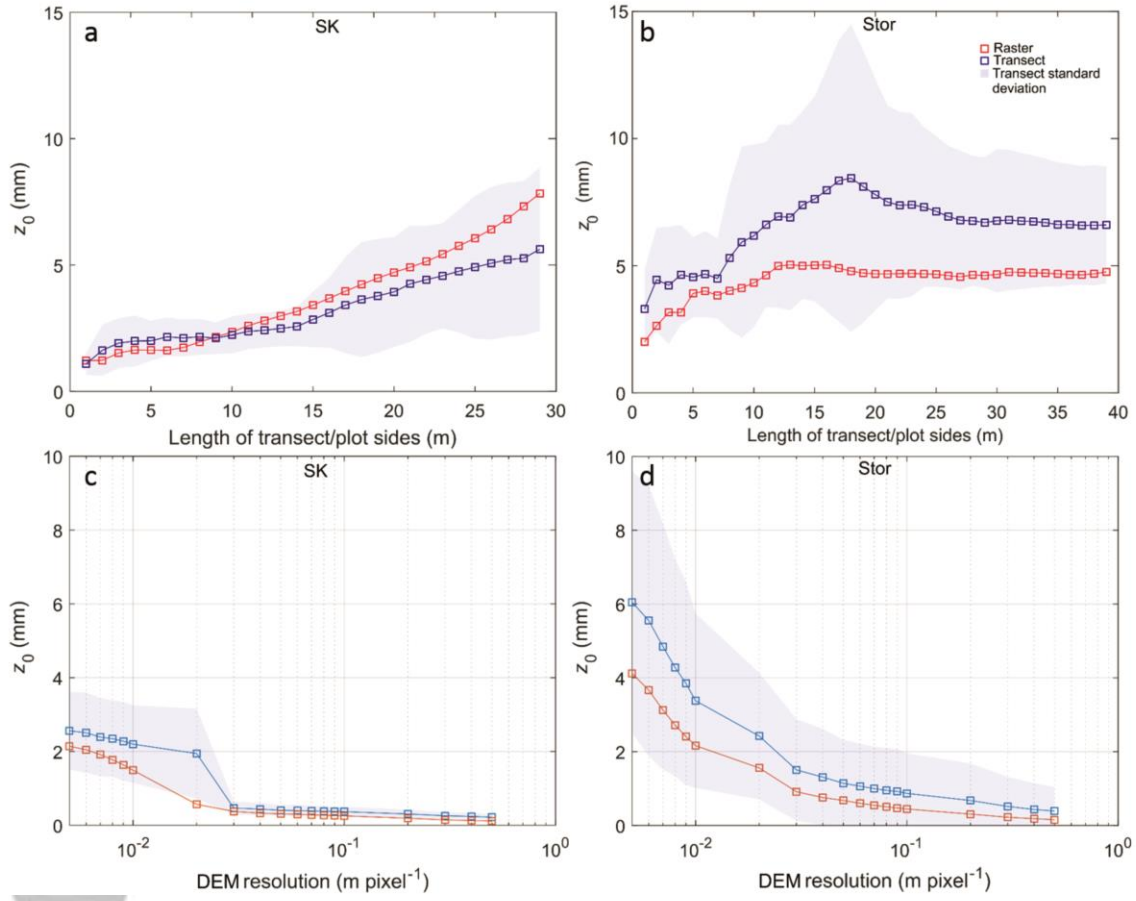

Fig. 6 Comparison of raster and transect z_0 with scale (a and b) and DEM resolution (c and d). The key in panel b is valid for all panels.